applied sciences

MDPI

Article

Numerical Study Investigating the Blasting Efficiency of the Long and Large-Diameter Uncharged Hole-Boring Method with Deck Charge Technique

Min-Seong Kim [1], Wan-Kyu Yoo [1], Wooseok Kim [1], Sungpil Hwang [1], Chang-Yong Kim [1] and Sean Seungwon Lee [2,*]

[1] Department of Geotechnical Engineering Research, Korea Institute of Civil Engineering and Building Technology, 283 Goyang-daero, Ilsanseo-gu, Goyang-si 10223, Republic of Korea
[2] Department of Earth Resources and Environmental Engineering, Hanyang University, 222 Wangsimni-ro, Seongdong-gu, Seoul 04763, Republic of Korea
* Correspondence: seanlee@hanyang.ac.kr

Abstract: The long and large-diameter uncharged hole-boring (LLB) method is a cut-blasting method used to reduce vibration induced by blasting. This method typically involves creating an uncharged hole with a 382 mm diameter and drilling 50 m in the tunnel excavation direction at a time. This method is reported to provide relatively good vibration reduction and with high blasting efficiency through short hole blasting compared to traditional cut methods. In this study, an advanced LLB method incorporating deck charge blasting was investigated to improve the blasting efficiency during long hole blasting. Numerical analysis was performed via ANSYS LS-DYNA to investigate the effectiveness of the deck charge technique. In the original LLB method, explosives were used to break the rocks more finely, and the fragmented rocks were concen trated at the end of the blast holes. On the contrary, the modified LLB, in which two-part explosives were loaded into the blast holes, is expected to push the fragmented rocks to the tunnel face more effectively than the original LLB method. Therefore, it is expected that the proposed LLB method combined with a deck charge technique can achieve superior blasting efficiency.

Keywords: cut method; LLB method; deck charge blasting method; 3D numerical simulation

Citation: Kim, M.-S.; Yoo, W.-K.; Kim, W.; Hwang, S.; Kim, C.-Y.; Lee, S.S. Numerical Study Investigating the Blasting Efficiency of the Long and Large-Diameter Uncharged Hole-Boring Method with Deck Charge Technique. *Appl. Sci.* **2023**, *13*, 2099. https://doi.org/10.3390/app13042099

Academic Editor: Arcady Dyskin

Received: 4 January 2023
Revised: 31 January 2023
Accepted: 3 February 2023
Published: 6 February 2023

1. Introduction

The drilling and blasting method is a popular rock excavation technique in civil engineering. However, it has the disadvantages of blasting-induced ground vibration and noise, the former of which is the most critical factor with regard to the surrounding structures [1,2]. Accordingly, the cut-blasting method is generally utilized to reduce vibration induced by blasting work [3,4], during which the fragmented rocks should be discharged in the first round of blasting toward empty space (excavation face) [5–7]. Traditional cut methods (V-cut method and cylinder-cut method) involve concentrating the explosives at the cut area to facilitate good discharge of the crushed rock; however, this may increase blast-induced vibration. Moreover, when long hole blasting of more than 2 m is conducted, it is difficult to discharge the crushed rock; thus, the blasting efficiency may decrease.

The long and large-diameter uncharged hole-boring (LLB) method is a cut-blasting method used to reduce vibration and involves creating an uncharged hole in the tunnel excavation direction [8]. This method utilizes an LLB hole that is horizontally drilled in the direction of the tunnel face. Notably, the diameter specification in South Korea is more than 250 mm. When a hole with a diameter of 362 mm is utilized, a 20–30% reduction in vibration efficiency can be achieved compared to that of traditional cut methods [9,10]. Moreover, in some cases, it has been reported that vibration can be reduced by up to approximately 79% compared to the V-cut method using multiple large-diameter uncharged holes [11]. The

LLB method is fundamentally advantageous for long and short hole blasting. Kim et al. [12] compared the blasting efficiency of the LLB method involving short hole blasting with that of the traditional cylinder-cut method through 3D numerical analysis. However, blast-induced vibration in one case was greater in the former than in the latter when the advance was 2 m [8], highlighting the necessity of minimizing vibration within the allowable value while maximizing the blasting efficiency.

We performed a 3D numerical study using ANSYS LS-DYNA to investigate rock fragmentation in the LLB method for long hole blasting. A Johnson–Holmquist (JH-2) constitutive material model was utilized to simulate the behavior of rock in dynamic states. In addition, an LLB method combined with a new deck charge technique (modified LLB method) was proposed to improve the blasting efficiency. Although investigating the blasting process and its efficiency in an actual tunnel construction site yields the highest accuracy, many risks are involved because most tunnel construction sites where the LLB method is applied are concentrated in urban areas, which are highly sensitive to blast-induced vibration and construction schedules. Therefore, the aim of this numerical study is to evaluate the blast ability of the modified LLB method before testing is performed in a tunnel construction site.

2. Rock Blasting Using Long and Large-Diameter Uncharged Holes

2.1. Introduction to the LLB Method

A schematic of the LLB mentioned above is shown in Figure 1. There are several advantages of the proposed method. First, a high-performance boring machine typically drills a 50 m length with hammer bit with a diameter of 382 mm in the tunnel excavation direction considering the entire preparation and boring time [13,14]. Accordingly, a free face is formed beyond the position of the explosives. Second, confining pressure is decreased by creating an LLB hole before blasting; thus, explosives around the uncharged hole can be reduced. Third, a relatively large space can be formed to move fragmented rocks after blasting; thus, additional free faces can be created. Fourth, geological conditions can be observed through a deeply drilled uncharged hole using an observation machine [15]. Finally, it helps to predict groundwater conditions ahead of the excavation face by investigating the amount of discharged groundwater.

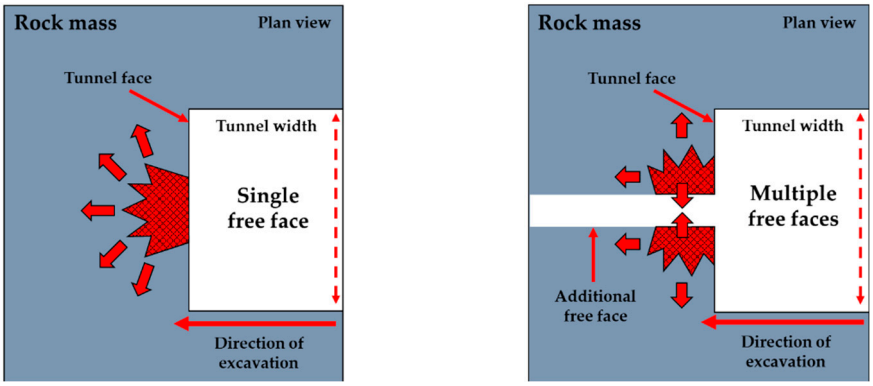

Figure 1. Comparison of (**a**) general tunnel blasting and (**b**) controlled tunnel blasting using the LLB method [8].

Figure 2 shows an example of the LLB method being applied to a tunnel construction site using a high-performance drilling machine. Drill rods with a length of 5 m are used to drill the LLB hole in the horizontal direction of the tunnel, and drilling up to a length of approximately 65 m is possible without any issues through the connection of each rod. One LLB hole is generally utilized (single LLB) to reduce vibration in urban areas. In addition, two or more LLB holes (multi-LLB) can be used, depending on the need for vibration reduction due to adjacent safety concerns.

Figure 2. Photograph of field application of the LLB method at a tunnel construction site located in South Korea.

2.2. Overview of Rock Fragmentation Process by Blasting

Figure 3 shows the process of rock fragmentation by rock blasting. When an explosive material detonates, a high-temperature gaseous product is generated, and the rock near the explosive is fractured. At the same time, a compressive stress wave generated by detonation propagates through the rock mass. Then, a tensile stress wave is generated due to the reflection of the compressive wave when the propagated compressive wave reaches a free surface, called a "Hopkinson effect" [16–19]. Rock material is known to be vulnerable to tensile rather than compressive conditions [20,21]; thus, tensile failure initiates around the free surface.

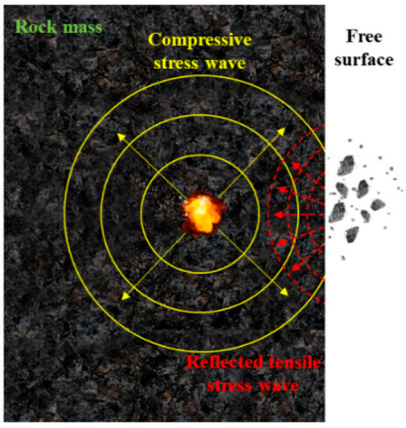

Figure 3. Effect of free surface in the rock blasting process.

However, the tunnel structure has only one free surface (tunnel excavation face). Therefore, it is the key to increasing the blast ability by artificially creating additional free faces in tunnel blasting. In this regard, a large-diameter uncharged hole formed deeper than a blast hole has the advantage of being able to effectively utilize the Hopkinson effect [12].

2.3. Comparison of Traditional Cut Methods and the LLB Method

Figure 4 shows a schematic of the three types of cut methods. The traditional V-cut method shown in Figure 4a is popularly applied to reduce blast-induced vibration. Additionally, it is suitable for short hole blasting. In contrast, the traditional cylinder-cut method shown in Figure 4b is commonly used for relatively long hole blasting. In this method, uncharged holes with a diameter of 102 mm are utilized to reduce blasting vibration. Traditional cut methods generally concentrate explosives at the end of the blast holes in the cut area to completely break rocks; this results in high blasting vibration.

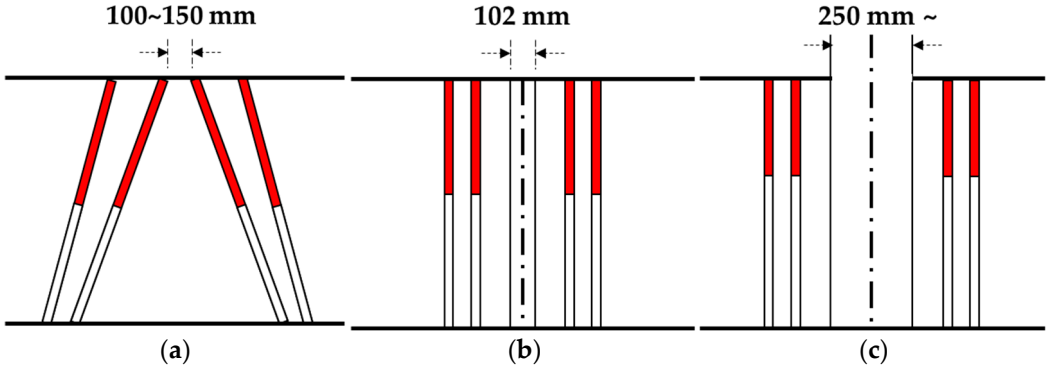

Figure 4. Schematic of the (**a**) V-cut method, (**b**) cylinder-cut method, and (**c**) LLB method.

The LLB method, which utilizes an LLB hole to maximize the vibration reduction efficiency, is illustrated in Figure 4c. The amount of explosives can be reduced by approximately 20% compared to the traditional cut method in the cut area because of a 382 mm diameter LLB hole; thus, blasting vibration can be decreased. Therefore, one of the advantageous features of this method is the increase in the advance per round due to tensile failure being induced in front of the explosives while minimizing the blasting vibration.

3. Numerical Analysis for the LLB Method

3.1. Analysis Model for the LLB Method

ANSYS LS-DYNA, a general-purpose finite-element software, was utilized to simulate the cut methods. This software has been broadly used to simulate complex dynamic and non-linear problems. It provides numerous material models and equations of state (EOS) to handle various material states under various conditions. The LLB method was modelled to study the mechanism of rock fragmentation during blasting, as shown in Figure 5. An arbitrary Lagrangian–Eulerian (ALE) solver was used to couple solid (rock) and fluid (explosives) materials [22].

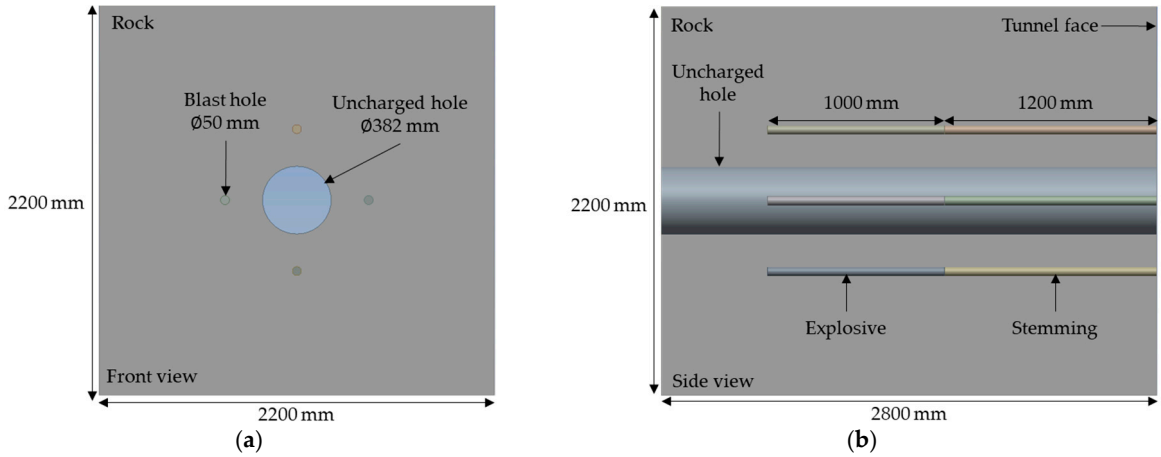

Figure 5. Geometry of the numerical simulation model for the LLB method: (**a**) front view and (**b**) side view.

The computing simulation was focused on the cut area, which has four blast holes (first round) located near a large-diameter uncharged hole, in order to investigate the initial failure behavior. The LLB method was modelled after an actual design pattern at a subway tunnel construction site. The blasting influence range was initially investigated by modelling 3000 × 3000 × 3000 mm (length, width, and depth, respectively) of rock materials, with 2000 × 2000 × 2800 mm ultimately used for simulation efficiency. The spacing between blast holes and LLB holes was 400 mm. The diameter and depth of the

blast holes were 50 mm and 2200 mm, respectively, and each blast hole has explosives with a depth of 1000 mm and the remaining 1200 mm was filled with stemming materials. In addition, the LLB hole was designed with a diameter of 382 mm from the tunnel face to the end of the rock. The LLB hole was designed with a dimeter of 382 mm until the end of the rock. All explosives were set to detonate simultaneously, and a non-reflecting boundary condition was set on all sides of the rock material except for the tunnel excavation face. The total number of meshes in this simulation model was 1,739,052, with a size of 20 mm.

3.2. Material Model and State Equation

A JH-2 constitutive model was utilized to simulate the behavior of rock mass in the dynamic state [23–25]. This model is widely used to simulate the behavior of brittle materials under dynamic conditions in LS-DYNA. This model is based on the relation of normalized equivalent stress and pressure. The JH-2 model reflects the pressure, damage evolution, fracture, strain-rate-dependent strength, and softening characteristics of the brittle materials [26]. It presents the strength and damage model and EOS, as shown in Figure 6. The strength model (Figure 6a) includes the intact (σ_i^*), damaged (σ^*), and fractured states (σ_f^*), which are calculated as follows:

$$\sigma_i^* = A(P^* + T^*)^N\left(1 + \mathrm{C}\cdot\ln\dot{\varepsilon}^*\right)\sigma^* = \sigma_i^* - D\left(\sigma_i^* - \sigma_f^*\right)\sigma_f^* = B(P^*)^M\left(1 + \mathrm{C}\cdot\ln\dot{\varepsilon}^*\right) \quad (1)$$

where σ_i^*, σ^*, and σ_f^* are the normalized intact, damaged, and equivalent stress, respectively; A, B, C, M, and N are material constants; P^* is the normalized hydrostatic pressure, which is calculated as $P^* = P/P_{HEL}$, where P and P_{HEL} are the hydrostatic pressure of the material and hydrostatic pressure at the Hugoniot elastic limit (HEL), respectively; and T^* is the normalized maximum tensile hydrostatic pressure, which can be computed as $T^* = T/P_{HEL}$, where T is the maximum tensile hydrostatic pressure. The strain rate can be expressed as $\dot{\varepsilon}^* = \dot{\varepsilon}/\dot{\varepsilon}_0$, where $\dot{\varepsilon}^*$ and $\dot{\varepsilon}_0$ are the actual equivalent strain rate and reference strain rate (1.0), respectively.

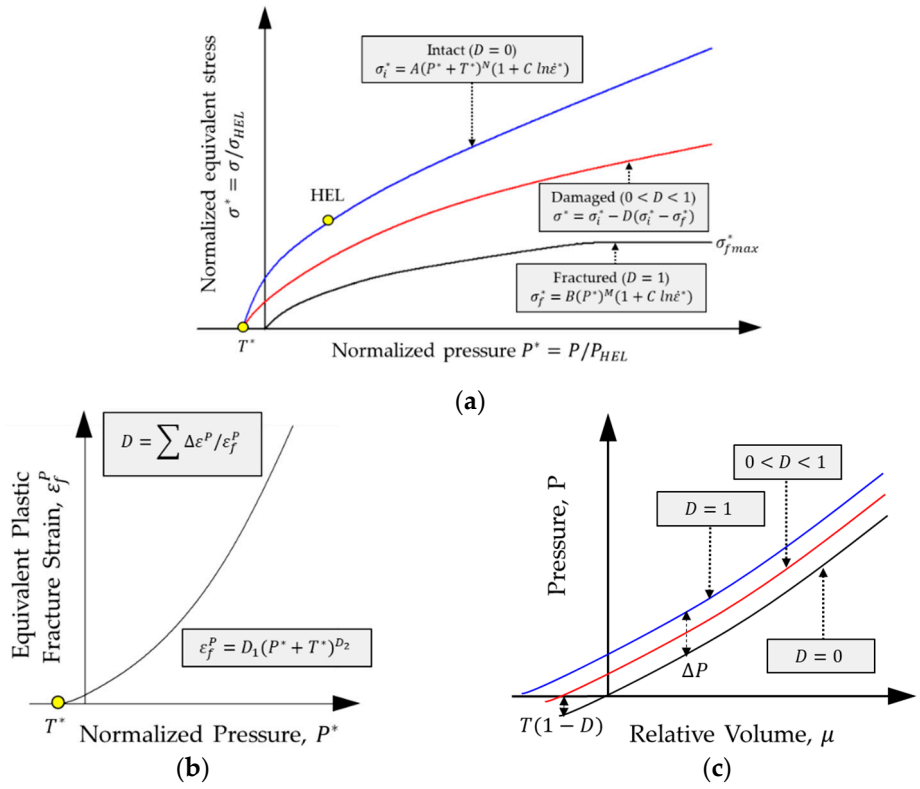

Figure 6. JH-2 material model: (**a**) strength model, (**b**) damage model, and (**c**) EOS [23].

In addition, damage accumulation, which exhibits non-linear behavior due to fracture generation, can be determined from the graph shown in Figure 6b. Depending on the pressure, the material status changes from intact to fractured states due to plastic deformation. In this case, the equivalent plastic strain can be expressed as follows [27]:

$$\varepsilon_f^p = D_1(P^* + T^*)^{D_2} \quad (2)$$

where ε_f^p is the equivalent plastic strain causing fracture under constant hydrostatic pressure; and P, D_1, and D_2 are damage constants. The damage is accumulated as the plastic deformation increase as follows:

$$D = \sum \Delta\varepsilon^p \varepsilon_f^p \quad (3)$$

where $\Delta\varepsilon^p$ is the equivalent plastic strain increment during an integration cycle.

Figure 6c shows the EOS of the JH-2 model, which describes the relationship of hydrostatic pressure and volumetric strain. The hydrostatic pressure before fractures and after damages begin to accumulate can be computed as follows:

$$P = K_1\mu + K_2\mu^2 + K_3\mu^3 \cdots (D = 0) P = K_1\mu + K_2\mu^2 + K_3\mu^3 + \Delta P \cdots (0 < D < 1) \quad (4)$$

where K_1, K_2, and K_3 are EOS constants, and K_1 is the initial bulk modulus of the material. The volumetric strain is $\mu = \rho/\rho_0 - 1$, where ρ and ρ_0 are the current and initial density, respectively. As damage begins to accumulate in the brittle material, the hydrostatic pressure (ΔP) is added to the polynomial EOS.

The parameters of granite, which is prevalent in South Korea, were input into the JH-2 model; the input parameters are summarized in Table 1 [28]. An element erosion technique was applied to simulate rock failure under blasting. Element deletion was set to initiate when the tensile stress induced by the free face exceeds the maximum tensile strength of the rock material.

Table 1. Input parameters of the JH-2 model.

Parameter	Value	Parameter	Value
Density (kg/m^3)	2560	Maximum normalized fractured strength	0.160
Shear modulus (GPa)	11.606	Hugoniot elastic limit (GPa)	4.500
Intact normalized strength parameter A	1.248	Pressure component at the Hugoniot elastic limit (GPa)	2.930
Fractured normalized strength parameter B	0.680	Fraction of elastic energy loss	1.000
Strength parameter C	0.005	Plastic strain to fracture D_1	0.008
Fractured strength parameter M	0.830	Plastic strain to fracture D_2	0.435
Intact strength parameter N	0.676	First pressure coefficient K1 (GPa)	10.720
Reference strain rate	1.000	Second pressure coefficient K2 (GPa)	−386
Maximum tensile strength (GPa)	0.015	Elastic constant K3 (GPa)	12,800

A Jones–Wilkins–Lee (JWL) EOS, which is broadly applied to define the relationship among pressure, volume, and energy of explosives, was used to simulate the blasting process [29], which can be computed as:

$$P = A\left(1 - \frac{\omega}{R_1 V}\right)^{-R_1 V} + B\left(1 - \frac{\omega}{R_2 V}\right)^{-R_2 V} + \frac{\omega}{V}E_0 \quad (5)$$

where P, E, and V are pressure, detonation energy per unit of volume, and relative volume, respectively; and A, B, R_1, R_2, and ω are the EOS coefficients. A HIGH_EXPLOSIVE_BURN

model, which can be coupled with the JWL EOS, was utilized to simulate the emulsion explosive material; the input parameters for the JWL EOS are summarized in Table 2 [30].

Table 2. Input parameters of JWL EOS and High_Explosive_Burn model.

JWL	**Parameter**	A (GPa)	B (GPa)	R_1	R_2	ω	E_0 (GPa/m^3/m^3)	V_0 (m^3/m^3)
	Value	276	8.44	5.215	2.112	0.501	3.868	1.0
High Explosives Burn	**Parameter**	RO (kg/m^3)		D (m/s)			P_{cj} (GPa)	
	Value	1180		5122			9.530	

where A, B, R_1, R_2, and ω are constants; E_0 and V_0 are the initial internal energy and initial relative volume, respectively; and RO, D, and P_{cj} are mass density, detonation velocity, and Chapman–Jouguet pressure, respectively.

Stemming is a material used to prevent the release of a high-pressure gaseous product induced by detonation by filling the remaining spaces after filling the explosive materials in the blast holes. The FHWA_SOIL model established by U.S. Federal Highway Administration [31] was used to model stemming. This model is known to be efficient in modelling the behavior of soil considering strain effects, strain softening, kinematic hardening, excessive pore–water effects, element deletion, and stability with no soil confinement [32]. The input parameters for the FHWA_SOIL model are listed in Table 3 [33,34].

Table 3. Input parameters of the FHWA_SOIL model.

Parameter	Value	Parameter	Value
Density (kg/m^3)	2350	Specific gravity	2.650
Density of water (kg/m^3)	1000	Skeleton bulk modulus (MPa)	0.153
Viscoplasticity parameter V_n	1.100	Viscoplasticity parameter γ_r	0.0
Maximum number of plasticity iterations	10.00	Minimum internal friction angle (radians)	0.063
Bulk modulus (MPa)	15.30	Shear modulus (MPa)	19.50
Peak shear strength angle (radians)	0.420	Cohesion (MPa)	0.011
Eccentricity parameter	0.700	Moisture content	6.200
Volumetric strain at the initial damage threshold	0.001	Strain hardening, percent of φ_{max} where non-linear effects start	10.00
Pore–water effects on bulk modulus PWD1	0.0	Pore–water effects on effective pressure PWD2	0.0
Void formation energy	10.00	Strain hardening, amount of non-linear effects	10.00

The large-diameter uncharged hole was modelled using a NULL model provided by the software. In addition, a void was modelled with a LINEAR_POLYNOMIAL EOS model, which is expressed by

$$P = C_0 + C_1\mu + C_2\mu^2 + C_3\mu^3 + \left(C_4 + C_5\mu + C_6\mu^2\right)E \quad (6)$$

where ρ is the mass density; C_0, C_1, C_2, C_3, C_4, C_5, and C_6 are constants; and E_0 is the initial internal energy. The input parameters for the NULL model are listed in Table 4 [35].

Table 4. Input parameters of the NULL model.

ρ (kg/m^3)	C_0	C_1	C_2	C_3	C_4	C_5	C_6	E_0 (MPa)
1.29	0.0	0.0	0.0	0.0	0.4	0.4	0.0	0.25

3.3. Analysis Results for the LLB Method

Figure 7 shows the numerical analysis results of applying the LLB method in three dimensions. The images show the rock (grey), large-diameter uncharged hole (grey), explosive (blue), and stemming (yellow). These results show the blasting process over time; the elements deleted by detonation of the explosives are shown in deep black.

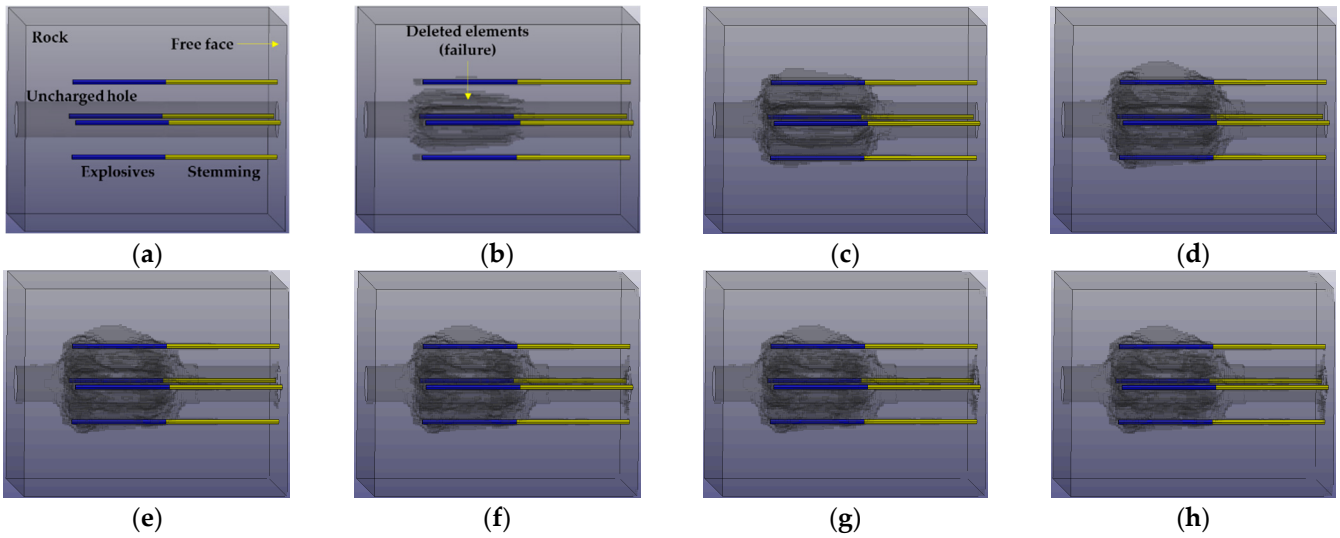

Figure 7. Results of numerical analysis of the LLB method: (**a**) 0 ms, (**b**) 0.5 ms, (**c**) 1.0 ms, (**d**) 1.5 ms, (**e**) 2.0 ms, (**f**) 2.5 ms, (**g**) 3.0 ms, (**h**) 3.5 ms.

The explosive materials detonate after 0 s, and rocks around the explosives are fragmented due to explosive energy. At the same time, a compressive stress induced by the detonations propagates through the rock. When the propagated compressive stress reaches the large-diameter uncharged hole (free surface), a tensile stress wave is generated due to the reflection of the compressive stress (Hopkinson effect). After 0.5 ms, rocks near uncharged holes begin to fragment due to their vulnerability to tensile stress. Thereafter, the extent of failure near the large-diameter uncharged hole increases. In addition, tensile failure was observed at the tunnel face due to the tensile stress wave generated by the reflection of the compressive stress wave at 2.0 ms.

Theoretically, the LLB method is more advantageous for long hole blasting due to the large-diameter uncharged hole formed at a greater depth than normal blasting holes. However, this analysis was focused on rock fragmentation in the area charged with explosives and is therefore limited to simulating flying rocks by gas pressure. Although a large-diameter uncharged hole is situated at the center of the explosives, large-scale rocks may not be sufficiently accommodated. In other words, the blast-induced high-pressure gaseous product may fail to sufficiently push away the remaining rocks.

4. Modified LLB Method with Deck Charge Technique

4.1. Concept behind the Modified LLB Method

The deck charge technique divides the explosives into multiple sections, with each blast hole having different detonation times. Therefore, reducing the charge per delay can simultaneously reduce the blasting vibration and increase the blasting efficiency [36–38]. Specifically, reductions in production and drilling costs have been reported to amount to 10–45% and 25%, respectively [39,40]. Moreover, the amount of explosives was reduced by 15–35%, along with improved blasting efficiency [41–43], and better breakage of rock was obtained using the air-deck charging technique in crater blasting [44]. Based on previous studies, it is understandable that the deck charge technique has a great advantage in improving rock blasting.

The newly proposed method is a modification of the LLB method that incorporates deck charge blasting to achieve efficient long hole blasting. The modified LLB method uses the same amount of explosives as the original LLB method, but the explosives are loaded in separate parts, as shown in Figure 8.

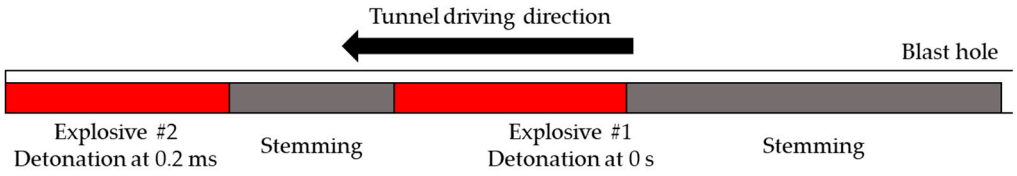

Figure 8. Schematic of charging pattern in the modified LLB method using the deck charge technique.

Figure 9 shows the predicted blasting process for the modified LLB method. When explosives #1 located near the excavation face are first detonated in stage 1, the crushed rocks are moved toward the free face (excavation face). This is important for creating additional free faces to facilitate the next round of blasting (stage 2). When explosives #2 located at the end of the blast holes are detonated in stage 3, the fragmented rocks are moved in stage 4 through the formed free face.

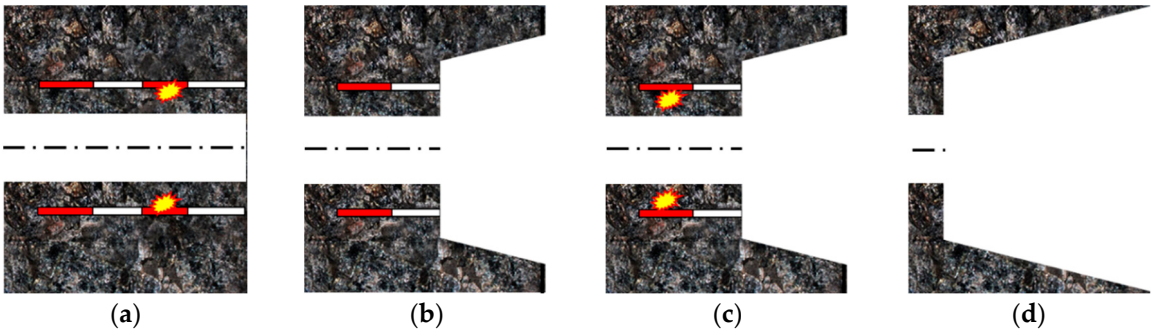

Figure 9. Expected rock fragmentation process of the proposed modified LLB method: (**a**) stage 1, (**b**) stage 2, (**c**) stage 3, (**d**) stage 4.

4.2. Analysis Model for Modified LLB Method

Figure 10 shows the simulation model for the advanced LLB method. This modified model is similar to the original LLB method except in charging patterns. The explosives were divided into two parts. Explosives #1 were loaded near the tunnel face and were set to detonate at 0 s, whereas explosives #2 were set to detonate at 20 ms (the generally used delay time in tunnel blasting). All basic settings of this simulation model were the same as the original LLB model, and the total number of meshes of this model was 1,740,056.

4.3. Analysis Results for Modified LLB Method

Figure 11 shows the computing simulation results for the modified LLB method. Explosives #1 detonated after 0 s, the rocks around the LLB hole were crushed, and the failure range increased over time. High-pressure gases can then push the crushed rocks to the large-diameter uncharged hole and excavation face (free faces). Meanwhile, new free faces corresponding to stage 2 were generated, as shown in Figure 9. Next, explosives #2 fragmented the remaining rocks after detonating at 20 ms, pushing the remaining crushed rocks to the large-diameter uncharged hole and newly created free faces.

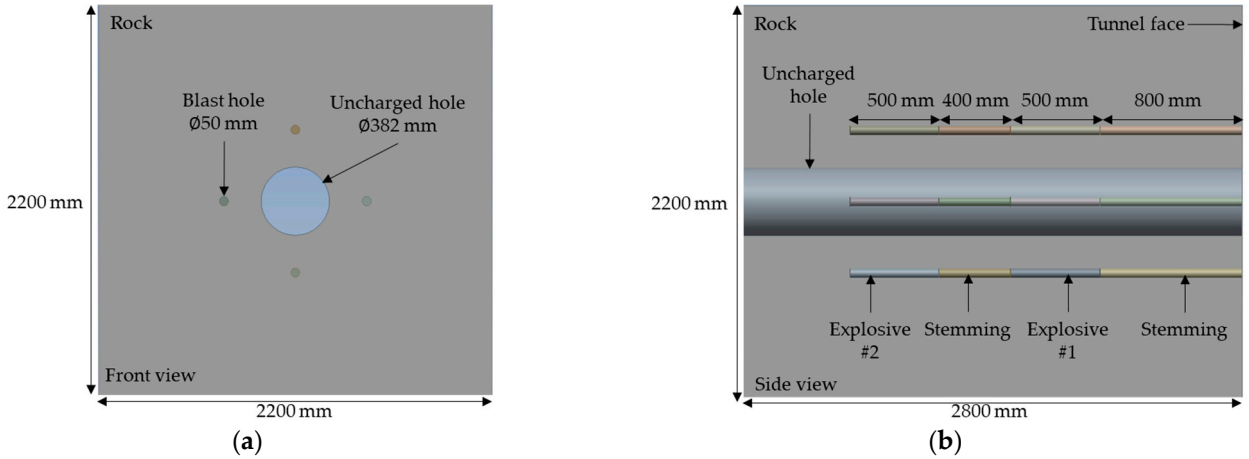

Figure 10. Geometry of the numerical simulation model for modified LLB method utilizing the deck charge technique: (**a**) front view and (**b**) side view.

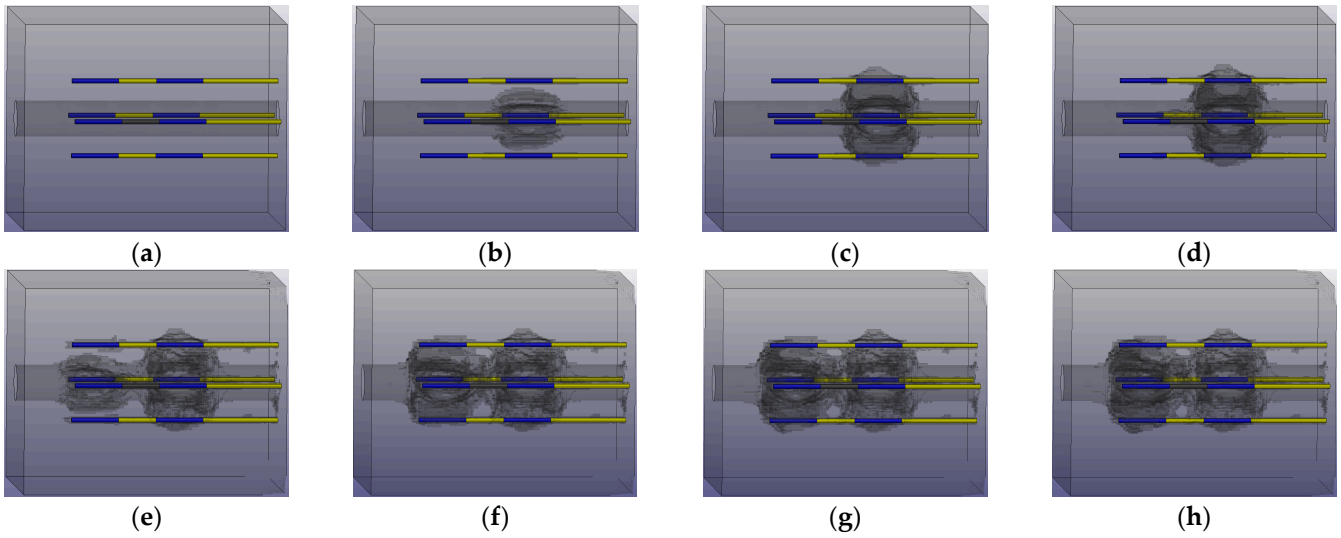

Figure 11. Numerical analysis results of the modified LLB method with deck charge technique: (**a**) 0 ms, (**b**) 0.5 ms, (**c**) 1.0 ms, (**d**) 1.5 ms, (**e**) 20.0 ms, (**f**) 20.5 ms, (**g**) 21.0 ms, (**h**) 21.5 ms.

Figure 12 shows a comparison of the failure ranges of each model in the last step. The total number of eroded elements for the original LLB method was 31,267, which was about 1.12 times lower than that in the modified LLB method, which was 35,050. The overall fragmented ranges of the modified LLB method were less than those in the original method; however, the explosives concentrated at the end of the blast hole were used to crush surrounding rocks into smaller pieces in the original LLB method. The advance per round in the original and modified model was 0.23 m and 0.19 m, respectively, which is attributable to the deeply formed large-diameter uncharged hole (free face) before blasting. The failure range of the modified LLB method was 1.03–1.10 m, which is up to 1.14 times smaller than that of the original model.

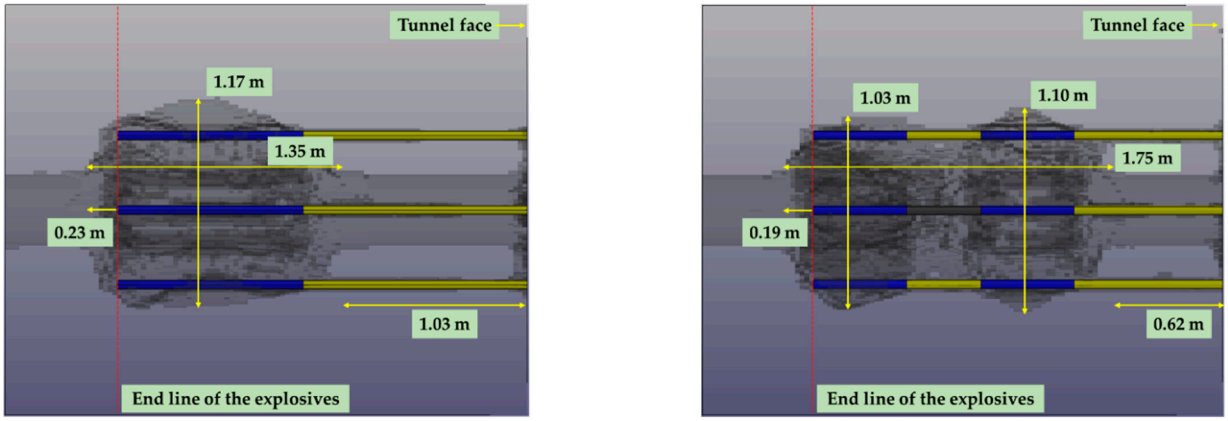

(**a**) (**b**)

Figure 12. Comparison of the failure patterns of (**a**) the original LLB method and (**b**) the modified LLB method using the deck charge technique.

Specifically, the distance between the final failure point and the tunnel face when applying the modified model was about 0.62 m, which is about 1.66 times shorter than that of the original model. Therefore, the explosives are expected to achieve a much better effect of pushing away fragmented rocks to the tunnel face when the modified model is used. In addition, the modified LLB method is of great significance in that it forms new free faces due to pre-detonation during the first stage. Overall, although the focus of this analysis model was on the cut area, the modified LLB method is expected to yield better blasting efficiency in the entire blasting process. Although, this method may be less constructable due to an increase in workload compared to the existing method, the increase in advance per round by improving blast ability using the modified LLB method is a significant advantage for the overall construction schedule.

5. Conclusions

In this study, a long and large-diameter uncharged hole-boring (LLB) method that can reduce vibration generated by blasting works was simulated to investigate its blasting efficiency for long hole blasting in tunnelling applications. ANSYS LS-DYNA software and a Johnson–Holmquist (JH-2) material model were used to simulate rock failure under dynamic conditions (blasting). In addition, a novel LLB method using a deck charge technique was simulated to assess the applicability of the method before applying it to an actual tunnel construction site.

As revealed in the 3D numerical analysis, the explosives concentrated at the end of the blast holes crushed the rocks around the explosives in the original LLB method during long hole blasting; specifically, the rocks were finely crushed. Accordingly, in the case of long hole blasting, the gaseous product may not adequately push the remaining rocks between the explosives and the tunnel face. However, in the modified LLB method applying a deck charge technique, the rocks were well crushed over a wider range than in the original method due to the explosives being loaded in two parts. In particular, this method can reduce the distance between the explosives and the tunnel face; thus, the gaseous product may presumably push away the remaining rocks efficiently in the direction of the tunnel face.

According to the analysis results, that the proposed method combining the LLB and deck charge technique can reduce blasting vibration and increase blasting efficiency, as well as advance per round, through the creation of additional free faces. Although the workload increases due to the deck charge technique, it is expected that more benefits can be obtained by reducing the overall construction period. Overall, this method is expected to be a cost-effective and eco-friendly alternative to reduce overall construction schedules and solve environmental problems. However, because these results were derived from

computing simulations, evaluation of the applicability and optimization of the design pattern of the proposed method are essential through field tests. This study is expected to support the application of the modified LLB method in high-risk tunnel construction sites where the LLB method is mainly applied.

Author Contributions: Conceptualization, S.S.L. and M.-S.K.; methodology, S.S.L. and M.-S.K.; software, M.-S.K.; validation, W.-K.Y., S.H., W.K. and C.-Y.K.; formal analysis, M.-S.K.; investigation, W.-K.Y. and W.K.; resources, S.H. and C.-Y.K.; data curation, M.-S.K.; writing—original draft, M.-S.K.; writing—review and editing, W.-K.Y., S.H., W.K., C.-Y.K. and S.S.L.; visualization, M.-S.K.; supervision, S.S.L.; project administration, S.S.L.; funding acquisition, S.S.L. All authors have read and agreed to the published version of the manuscript.

Funding: This work is supported by the Korea Agency for Infrastructure Technology Advancement (KAIA) grant funded by the Ministry of Land, Infrastructure and Transport (Grant 22UUTI-C157786-03).

Institutional Review Board Statement: Not applicable.

Informed Consent Statement: Not applicable.

Data Availability Statement: The data used to support the findings of this study are included within the article.

Conflicts of Interest: The authors declare no conflict of interest.

References

1. Langefors, U.; Kihlstrom, B. *The Modern Technique of Rock Blasting*; Wiley: New York, NY, USA, 1963.
2. Yu, Z.; Shi, X.Z.; Zhou, J.; Chen, X.; Qiu, X.Y. Effective assessment of blast-induced ground vibration using an optimized random forest model based on a harris hawks optimization algorithm. *Appl. Sci.* **2020**, *10*, 1403. [CrossRef]
3. Singh, S.P. Mechanism of cut blasting. *Trans. Inst. Min. Metall.* **1995**, *104*, A134–A138.
4. Gao, P.F.; Zong, Q.; Cheng, B.; Wang, H.B.; Xu, Y.; Zhang, B.B. Investigation on cutting blasting efficiency of hard rock tunnels under different charge diameters. *Appl. Sci.* **2022**, *19*, 9906. [CrossRef]
5. Zare, S.; Bruland, A. Comparison of tunnel blast design models. *Tunn. Undergr. Space Technol.* **2006**, *21*, 533–541. [CrossRef]
6. Xie, L.X.; Lu, W.B.; Zhang, Q.B.; Jiang, Q.H.; Chen, M.; Zhao, J. Analysis of damage mechanisms and optimization of cut blasting design under high in-situ stresses. *Tunn. Undergr. Space Technol.* **2017**, *66*, 19–33. [CrossRef]
7. An, H.; Song, Y.; Yang, D. Experimental study of the effect of rock blasting with various cutting forms for tunnel excavation using physical model tests. *Arch. Civ. Eng.* **2021**, *67*, 599–618. [CrossRef]
8. Kim, M.S.; Lee, S.S. The efficiency of large hole boring (MSP) method in the reduction of blast-induced vibration. *Appl. Sci.* **2021**, *11*, 1814. [CrossRef]
9. Beak, J.H.; Beak, S.H.; Han, D.H.; Won, A.R.; Kim, C.S. A study on the design of PLHBM. *Explos. Blasting* **2012**, *30*, 66–76.
10. Choi, Y.H.; Kim, M.S.; Lee, S.S. Prediction of vertical alignment of the MSP borehole using artificial neural network. *KSCE J. Civ. Eng.* **2022**, *26*, 4330–4337. [CrossRef]
11. Choi, H.B.; Han, D.H.; Ki, K.C. A study on the decay effect of ground vibration based on the number of PLHBM holes in gneiss area. *Explos. Blasting* **2016**, *34*, 1–9.
12. Kim, M.S.; Kim, C.Y.; Song, M.K.; Lee, S.S. Assessment of the blasting efficiency of a long and large-diameter uncharged hole boring method in tunnel blasting using 3D numerical analysis. *Sustainability* **2022**, *14*, 13347. [CrossRef]
13. Kim, M.S.; Lee, S.S. Investigation of geological conditions beyond the excavation face using a MSP boring data monitoring system. *Int. J. Rock Mech. Min. Sci.* **2022**, *157*, 105161–105171. [CrossRef]
14. Kim, M.S.; Lee, J.K.; Choi, Y.H.; Kim, S.H.; Jeong, K.W.; Kim, K.L.; Lee, S.S. A study on the optimal setting of large uncharged hole boring machine for reducing blast-induced vibration using deep learning. *Explos. Blasting* **2020**, *38*, 16–25.
15. Kim, M.S.; Jung, J.H.; Lee, J.K.; Park, M.S.; Bak, J.H.; Lee, S.S. Development and application of large-diameter cut-hole exploration system for assessment of the geological condition beyond NATM tunnel face. *Tunn. Undergr. Space* **2021**, *31*, 1–9.
16. Hopkinson, B. A method of measuring the pressure produced in the detonation of high explosives or by the impact of bullets. *Proc. R. Soc. A Math. Phys. Eng. Sci.* **1914**, *89*, 411–413. [CrossRef]
17. Kolsky, H. Stress wave in solids. *J. Sound Vib.* **1964**, *1*, 88–110. [CrossRef]
18. Cho, S.H.; Kaneko, K. Influence of the applied pressure waveform on the dynamic fracture processes in rock. *Int. J. Rock Mech. Min.* **2004**, *41*, 771–784. [CrossRef]
19. Chai, S.B.; Li, J.C.; Zhang, Q.B.; Li, H.B.; Li, N.N. Stress wave propagation across a rock mass with two non-parallel joints. *Rock Mech. Rock Eng.* **2016**, *49*, 4023–4032. [CrossRef]
20. Kutter, H.K.; Fairhurst, C. On the fracture process in blasting. *Int. J. Rock Mech. Min. Sci. Geomech. Abstr.* **1971**, *8*, 189–202. [CrossRef]

21. Cheng, B.; Wang, H.B.; Zong, Q.; Xu, Y.; Wang, M.X.; Zhu, N.N. Study on the novel technique of straight hole cutting blasting with a bottom charged central hole exploded supplementally. *Arab. J. Geosci.* **2021**, *14*, 2838–2867. [CrossRef]
22. Alia, A.; Souli, M. High explosive simulation using multi-material formulations. *Appl. Therm. Eng.* **2006**, *26*, 1032–1042. [CrossRef]
23. Johnson, G.R.; Holmquist, T.J. A computational constitutive model for brittle materials subjected to large strains, high strain rates and high pressures. In *Shock Wave and High-Strain-Rate Phenomena in Materials*; Meyers, M., Murr, L., Staudhammer, K., Eds.; CRC Press: Boca Raton, FL, USA, 1992; pp. 1075–1081.
24. Johnson, G.R.; Holmquist, T.J. An improved computational constitutive model for brittle materials. *AIP Conf. Proc.* **1994**, *309*, 981–984. [CrossRef]
25. Banadaki, M.M.D.; Mohanty, B. Numerical simulation of stress wave induced fractures in rock. *Int. J. Impact. Eng.* **2012**, *40–41*, 16–25. [CrossRef]
26. Min, G.J. GPGPU-Accelerated 3D Dynamic Fracture Process Analysis and Its Application to High Strain-Rate Fracturing in Geomaterials. Ph.D. Thesis, Jeonbuk National University, Jeonju, Republic of Korea, 2021.
27. Baranowski, P.; Kucewicz, M.; Gieleta, R.; Stankiewicz, M.; Konarzewski, M.; Bogusz, P.; Pytlik, M.; Malachowski, J. Fracture and fragmentation of dolomite rock using the JH-2 constitutive model: Parameter determination, experiments and simulations. *Int. J. Impact Eng.* **2020**, *140*, 103543–103555. [CrossRef]
28. Wang, J.X.; Yin, Y.; Lu, C.W. Johnson-Holmquist-II(JH-2) constitutive model for rock materials: Parameter determination and application in tunnel smooth blasting. *Appl. Sci.* **2018**, *8*, 1675. [CrossRef]
29. Lee, E.L.; Horning, H.C.; Kury, J.W. A Diabatic Expansion of High Explosives Detonation Products. TID4500-UCRL 50422; Lawrence Livermore National Laboratory, University of California: Livermore, CA, USA, 1968.
30. Hansson, H. *Determination of Properties for Emulsion Explosives Using Cylinder Expansion Tests and Numerical Simulation. Swebrec Report*; Swedish Blasting Research Centre: Stockholm, Sweden, 2009.
31. Lewis, B.A. *Manual for LS-DYNA Soil Material Model 147*; Federal Highway Administration: McLean, VA, USA, 2004.
32. Livermore Software Technology, *LS-DYNA Keyword User's Manual—Volume II*; Livermore, CA, USA, 2020.
33. Koneshwaran, S.; Thambiratnam, D.P.; Gallage, C. Blast response of segmented bored tunnel using coupled SPH-FE method. *Structures* **2015**, *2*, 58–71. [CrossRef]
34. Baranowski, P.; Mazurkiewicz, L.; Malachowski, J.; Pytlik, M. Experimental testing and numerical simulations of blast-induced fracture of dolomite rock. *Meccanica* **2020**, *55*, 2337–2352. [CrossRef]
35. Zhai, X.W.; Wu, S.B.; Wang, K.; Chen, X.K.; Li, H.T. A novel design of rescue capsule considering the pressure characteristics and thermal dynamic response with thermomechanical coupling action subjected to gas explosion load. *Shock Vib.* **2017**, *25*, 5261309. [CrossRef]
36. Jhanwar, J.C.; Cakraborty, A.K.; Anireddy, H.R.; Jethwa, J.L. Application of air decks in production blasting to improve fragmentation and economics of an open pit mine. *Geotech. Geol. Eng.* **1999**, *17*, 37–57. [CrossRef]
37. Cheng, R.H.; Zhou, Z.L.; Chen, W.S.; Hao, H. Effects of axial air deck on blast-induced ground vibration. *Rock Mech. Rock Eng.* **2022**, *55*, 1037–1053. [CrossRef]
38. Chen, Y.X.; Chen, J.; Wang, P.F.; Zhou, M.; Yang, H.X.; Li, J.Y. Design method of blasthole charge structure based on lithology distribution. *Sci. Rep.* **2021**, *11*, 24247–24261. [CrossRef] [PubMed]
39. Chiappetta, R.F.; Memmele, M.E. Analytical high-speed photography to evaluate air-decks, stemming retention and gas confinement in pre-splitting reclamation and gross motion studies. In Proceedings of the Second International Symposium on Rock Fragmentation by Blasting, Bethel, CT, USA, 23−26 August 1987.
40. Bussey, J.; Borg, D.G. Pre-splitting with the new air-deck technique. In Proceedings of the 14th Conference on Explosive and Blasting Technique, Explosive Engineers Annual Meeting, Anaheim, CA, USA, 31 January–5 February 1988.
41. Mead, D.J.; Moxon, N.T.; Danell, R.E.; Richardson, S.B. The use of air-decks in production blasting. In Proceedings of the Fourth International Symposium on Rock Fragmentation by Blasting, Vienna, Austria, 5−8 July 1993.
42. Rowlands, M.D. Separating explosive charges with air gaps to improve fragmentation whilst reducing explosive usage. In Proceedings of the Second Conference on Large Open Pit Mining, Latrobe Valley, VIC, Australia, 3−6 April 1989.
43. Jhanwar, J.C.; Jethwa, J.L. The use of air decks in production blasting in an open pit coal mine. *Geotech. Geol. Eng.* **2000**, *18*, 269–287. [CrossRef]
44. Singh, T.N.; Sazid, M.; Saharan, M.R. A study to simulate air deck crater blast formation—A numerical approach. In Proceedings of the 7th Asian Rock Mechanics Symposium, Seoul, Republic of Korea, 15−19 October 2012.